Numerical Analysis of Nonequilibrium Electron Transport in AlGaAs/InGaAs/GaAs Pseudomorphic MODFET's

TAHUI WANG AND CHENG-HSIANG HSIEH

Abstract—**Nonequilibrium electron transport in the InGaAs pseudomorphic MODFET's has been analyzed with the moment equations approach. In our model, the momentum and energy balance equations for the two-dimensional electrons in the InGaAs channel are solved with relaxation times generated from a Monte Carlo simulation. The two-dimensional electron wave functions and the quantized states energies in the InGaAs quantum well are calculated exactly from the Schrödinger equation along the direction perpendicular to the quantum well. Also included is a two-dimensional Poisson equation solver. In the calculation, all of the equations are solved iteratively until a self-consistent solution is achieved. The simulation result for a realistic device structure with a 0.5-μm recessed gate shows a significant overshoot velocity of 4.5 $\times$ 10^7 cm/s at a drain bias of 1.0 V. Electron temperature reaches a peak value of around 2500 K under the gate. In energy transport, the diffusive component of the energy flux is found to be dominant in the high-field region.**

I. Introduction

IN RECENT YEARS, submicrometer AlGaAs/InGaAs/GaAs pseudomorphic modulation doped field-effect transistors (MODFET) [1] have attracted considerable interest because of their potential for ultra-high speed applications. The conducting channel of a pseudomorphic MODFET is a thin InGaAs layer sandwiched between a doped AlGaAs layer and an unintentionally doped GaAs buffer. The inclusion of the InGaAs layer is to provide better electron confinement and superior electron transport characteristics. In these devices, the sheet concentration of the two-dimensional electron gas (2DEG) is increased over comparable AlGaAs/GaAs structures due to the increase of the conduction band-edge discontinuities at the heterojunctions. Electron mobility and steady-state saturation velocity in InGaAs are intrinsically higher than those in GaAs. Furthermore, owing to a larger Γ valley to L valley energy separation, the intervalley scattering in InGaAs occurs at relatively higher electron energies and therefore a larger non-steady-state electron overshoot velocity [2], [3] is also expected in InGaAs. A higher electron velocity and a larger 2DEG density have lent these devices an excellent candidate for high-speed digital and analog applications. The cut-off frequencies of the 0.25-μm pseudomorphic MODFET's have been demonstrated to be around 100 GHz [4].

In order to study the charge-modulation behavior of the InGaAs potential well in which the quantum-size effects are prominent, it is necessary to solve the Schrödinger equation and the Poisson equation self-consistently with various effects taken into account, for example, many-body exchange force, donor neutralization, and wave-functions penetration into the large bandgap materials. The pseudomorphic MODFET's have been studied by Ando and Itoh [5] using this approach. However, their charge control model is subject to some limitations. i) The Poisson equation is solved only one-dimensionally. Hence, Ando and Itoh's model is valid only in the low-field region of the channel where the gradual channel approximation (GCA) is appropriate. ii) The parasitic or access regions of the device are not included, which are of importance to the device performance especially in the submicrometer domain. iii) The temperature of the 2DEG has to be assumed equal to the lattice temperature (300 K). The first two limitations can be removed by solving the two-dimensional Poisson equation in the entire device. The third one involves the problem of electron transport and one has to use a more advanced transport model.

Many authors [6], [7] have employed the continuity equation and the current equation together with a field-dependent mobility model in their analyses of the electron transport in the MODFET's. Based on the assumption that the electron drift velocity is always in equilibrium with the local electric field, these conventional transport models lack the capability to treat the nonstationary properties correctly. Consequently, ensemble Monte Carlo (EMC) methods [8], [9] have been developed to solve the electron distribution function in the MODFET's directly from the first-principle Boltzmann transport equation (BTE). However, the EMC methods require tremendous computer resources to track simultaneously a large number (typically, several thousands) of electron trajectories in both real and momentum space. The third category of approaches consists of the momentum and energy balance

Manuscript received November 14, 1989; revised March 7, 1990. This work was supported by the National Science Council under Contract NSC77-0404-E0009-25. The review of this paper was arranged by Associate Editor S. E. Laux.

T. Wang is with the Institute of Electronics, National Chiao-Tung University, Hsin-Chu, Taiwan, Republic of China.

C. H. Hsieh was with the Institute of Electronics, National Chiao-Tung University, Hsin-Chu, Taiwan Republic of China. He is now with Winbond Electronics Corp.

IEEE Log Number 9036874.

equations derived from the moments of the BTE [10]. In addition to electron concentration, electron velocity and temperature are also involved. In these methods, it is a set of partial differential equations rather than a function of the local electric field to determine the local carrier energy and velocity. Although these models are not as rigorous as the EMC model, they provide a satisfactory description of the nonstatic characteristics of electron dynamics. In order to keep the most important features of velocity overshoot without consuming too much CPU time, we have developed a moment equations model for the analysis of electron transport in the pseudomorphic MODFET's.

A realistic device structure with a recessed gate is used throughout this study. Our model includes the one-dimensional continuity equation, momentum balance and energy balance equations of electrons in the quantum well with momentum and energy relaxation times generated from the Monte Carlo simulations. The one-dimensional analysis along the direction parallel to the quantum well for electron transport is appropriate since the InGaAs channel is sufficiently thin and strong electron confinement always exists at both sides of the InGaAs channel. The wave functions and the quantized state energies of the 2DEG are calculated exactly from the Schrödinger equation along the direction perpendicular to the quantum well. Also included is a two-dimensional Poisson equation solver to provide an electric field distribution for transport calculation and a band-edge profile used in the Schrödinger equation. Electron temperature instead of lattice temperature is employed to determine the electron distribution in the quantized states. All of the above mentioned equations are iteratively solved until a self-consistent solution is achieved.

In the following sections, the details of our model and the simulation procedures will be described and the basic physics of the device operation will be analyzed in depth based on the calculated results.

II. Physical Model

A. Electron Transport Equations

The investigated device structure is illustrated schematically in Fig. 1. In order to describe the two-dimensional (2D) electron dynamics in the channel in terms of electron concentration, velocity, and temperature by the balance equations, one can multiply the BTE by appropriate functions of electron velocity and integrate it over the momentum space using the relaxation time approximation for the collision integral [11]. The moments of the BTE along the channel direction are derived as follows:

i) The continuity equation

$$\frac{\partial}{\partial x}(n_s v) = 0. \tag{1}$$

ii) The momentum balance equation

$$\frac{qF}{m^*} - \frac{v}{\tau_m(E)} - \frac{k}{n_s m^*}\frac{\partial}{\partial x}(n_s T) - v\frac{\partial v}{\partial x} = 0. \tag{2}$$

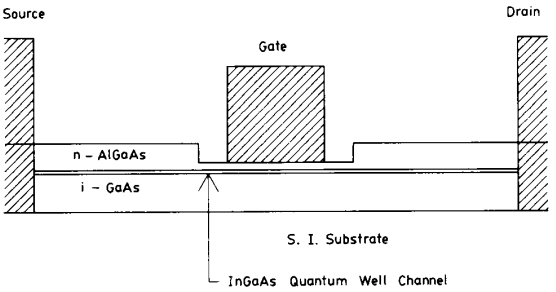

Fig. 1. Schematic representation of an InGaAs pseudomorphic MODFET.

iii) The energy balance equation

$$qvF - \frac{E - E_0}{\tau_e(E)} - v\frac{\partial}{\partial x}(E + kT) - \frac{1}{n_s}\frac{\partial Q}{\partial x} = 0 \tag{3}$$

where

$n_s(x)$ sheet electron concentration,
$v(x)$ average electron velocity,
$T(x)$ electron temperature,
$E(x)$ average electron energy,
$F(x)$ electric field,
k Boltzmann constant,
m^* effective electron mass,
E_0 equilibrium electron thermal energy,
$Q(x)$ diffusive component in the energy flux.

The momentum relaxation time τ_m and the energy relaxation time τ_e are assumed to be functions of average electron energy E. In (2), $n_s kT$ is interpreted as the electron gas pressure. Hence

$$\frac{k}{n_s m^*}\frac{\partial}{\partial x}(n_s T)$$

expresses the deceleration due to the force exerted by the gradient of electron gas pressure. $v(\partial v/\partial x)$ is identified as the acceleration of electrons. In our one-dimensional (1D) case, the electron energy flux is written as $n_s v(E + kT) + Q$ in which $n_s v(E + kT)$ is the convective component, or the energy drift, and Q is the diffusive component, or the energy diffusion. Therefore, the last two terms in (3) describe the power conveyed by an energy flow gradient. The readers should be reminded that Q in (3) is defined to reflect the third central moment or the skewness of the distribution function [12]. Assuming a drifted Maxwellian distribution function, many authors simply neglected this energy diffusion term in their balance equations [13]-[15]. The importance of keeping Q in (3) will be discussed later. We adopt an approximation for Q suggested in [12] to avoid the coupling between (3) and other higher order moment equations.

$$Q = -\frac{5k^2 n_s \tau_m(E) T}{2m^*}\frac{\partial T}{\partial x}. \tag{4}$$

In this equation

$$\frac{5k^2 n_s \tau_m(E)T}{2m^*}$$

expresses the thermal conductivity of the electron gas according to the Wiedemann–Franz law [16], [17] in which the r value is chosen to be 0 for the polar optical phonon scattering. Slightly different forms of Q have been used by Widiger *et al.* [18] and Azroff [19]. It should be pointed out that one can derive $E = \frac{1}{2} m^* v^2 + kT$ in (3) for the 2D electron transport in a single subband. However, since the present model includes multiple subbands and electron transitions between different subbands are possible, we still choose $E = \frac{1}{2} m^* v^2 + \frac{3}{2} kT$ as an approximation.

B. Momentum and Energy Relaxation Times

To obtain τ_m and τ_e as the functions of electron energy E, the ensemble Monte Carlo simulations have been performed for bulk $In_xGa_{1-x}As$ ($x = 0.15$) at 300 K employing the material parameters suggested by Brennan *et al.* [20]. In our calculation, principle scattering mechanisms such as polar optical phonon scattering and intervalley phonon scattering are incorporated. The effect of impurity scattering is intentionally removed because the ionized donors are separated from the conducting channel by an undoped spacer layer in a MODFET structure. The 2D quantization effect is neglected in the calculation of the relaxation times. This is justified by the Monte Carlo simulation in GaAs performed by Yokoyama *et al.* [21]. Yokoyama's result indicates that the low-field 2D electron mobility at 300 K is about 8100 $cm^2/V \cdot s$, only slightly different from the bulk electron mobility of 8000 $cm^2/V \cdot s$ in intrinsic GaAs. Calculated steady-state electron energy and drift velocity versus electric field are drawn in Fig. 2. In addition, the results in bulk GaAs are also shown for comparison. These data are transformed into $\tau_m(E)$ and $\tau_e(E)$ in Fig. 3.

The relaxation times have been used in a study of the transient response of the electron drift velocity [3] to an electric field step in homogeneous GaAs. In this study, the transient forms of (2) and (3) without the spatial derivatives are derived. The transient velocity $v(t)$ is solved using the Euler method. Fig. 4 directly compares the results from the balance equations and from a Monte Carlo simulation. An excellent agreement is achieved. It is evident that the velocity overshoot phenomena can be successfully analyzed with these balance equations. As a matter of fact, electron transport takes place in multiple valleys in GaAs. Our model actually assumes an equivalent single valley. This approximation is appropriate since the effects of valley transfer (Gunn effects) and band nonparabolicity have been simulated in the Monte Carlo calculations. Thus the multiple-valley transport behavior is incorporated in this "equivalent" single-valley model through the use of the Monte Carlo generated relaxation time. Consistency obtained in Fig. 4 confirmed that the multiple valley models [11] or the energy-dependent effective mass [15] in the balance equations approach are not absolutely necessary.

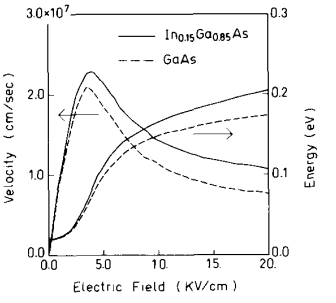

Fig. 2. Monte Carlo calculated steady-state electron energy and drift velocity versus electric field in $In_{0.15}Ga_{0.85}As$ and in GaAs.

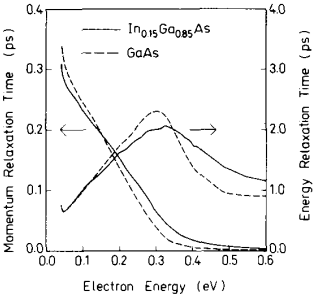

Fig. 3. Momentum and energy relaxation times as functions of electron energy calculated from the Monte Carlo simulation in the $In_{0.15}Ga_{0.85}As$ and in GaAs.

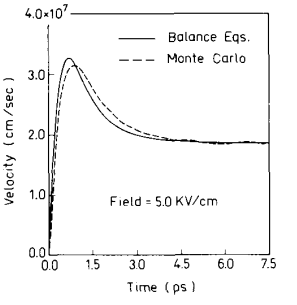

Fig. 4. Transient response of the electron velocity in GaAs to an electric field step of 5.0 kV/cm starting at time = 0.0 ps. The solid line represents the balance equations result and the dashed line is generated from a Monte Carlo simulation.

C. Quantization Effects of the Two-Dimensional Electrons

As illustrated in Fig. 5, a self-consistent conduction band-edge profile and the 2DEG wave functions are solved from the mutually coupled Poisson and Schrödinger equations in our model. The spatial distribution of the 2D electrons is deduced from the electron wave functions. The Schrödinger equation for the envelope wave function $\psi_i(x,$

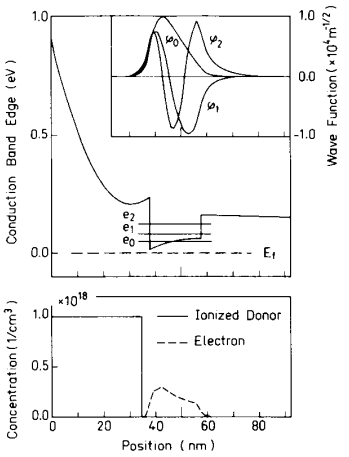

Fig. 5. Self-consistent wave functions, conduction band edge, and charge density plotted as functions of position in the direction perpendicular to the quantum well. e_0, e_1, and e_2 are the lowest three eigenenergies and φ_0, φ_1, and φ_2 are the corresponding wave functions. At this cross section, almost all of the donors are ionized.

y) in the ith subband at x (x is defined along the channel direction)

$$\left[-\frac{\hbar^2}{2m^*}\frac{\partial^2}{\partial y^2} + V(x, y)\right]\psi_i(x, y) = e_i(x)\psi_i(x, y) \quad (5)$$

and

$$V(x, y) = -q\phi(x, y) + V_h(y) + V_{ex}(x, y) \quad (6)$$

where $2\pi\hbar$ is Planck's constant, $e_i(x)$ is the ith eigenenergy at x, $V_h(y)$ is the heterojunction conduction band discontinuity, and $V_{ex}(x, y)$ is the local exchange-correlation potential. Here, we use an analytic parameterization for V_{ex} [22]. The inclusion of the exchange force reduces the eigenenergies. The image potential energy is ignored because the dielectric constants differ so little in the AlGaAs/InGaAs/GaAs systems. In our quantization calculations, (5) is solved for the lowest three eigenstates ($i = 0$, 1, and 2). For electron temperature at 300 K, more than 90% of total electrons are populated in these three subbands. Beyond the third eigenstate, the energy separation between two consecutive eigenstates is comparable to or less than the thermal energy kT, in our case. The thermal broadening may smear out the energy quantization effect. Therefore, electrons at higher states are treated as three-dimensional (3D) bulk electrons. The distributions of the 2D and the 3D bulk electrons are determined by an equivalent electron temperature, which is a variable in the transport equations.

The wave functions solved from (5) are used to calculate the charge density in the 2D Poisson equation, i.e.,

$$\nabla \cdot [\epsilon(x, y)\nabla\phi(x, y)] = -q[N_D^+(x, y) - n(x, y)] \quad (7)$$

where $\epsilon(x, y)$ is the position-dependent dielectric constant and $n(x, y)$ is the density of the electrons.

$$n(x, y) = \sum_{i=0}^{m} n_i(x)\left|\psi_i(x, y)\right|^2 + n_{3d}(x, y) \quad (8)$$

where m is the index of the highest subband in which the quantization effects are considered. In our model, m is chosen to be 2. $n_i(x)$ is the 2DEG sheet concentration in the ith subband and $n_{3d}(x, y)$ represents the concentration of the 3D bulk electrons. They are expressed in the following:

$$n_i(x) = \frac{m^*kT(x)}{\pi\hbar^2}\ln\left[1 + \exp\left(\frac{E_f(x) - e_i(x)}{kT(x)}\right)\right] \quad (9)$$

$$n_{3d}(x, y) = N_c(y)2(\pi)^{-1/2}H(u(x, y), s(x, y)) \quad (10)$$

where E_f is the quasi-Fermi level and N_c is the effective density of states of the conduction band. $u(x, y)$, $s(x, y)$, and $H(u, s)$ are defined below

$$u(x, y) \equiv \begin{cases} \dfrac{e(x) - E_c(x, y)}{kT}, \\ \qquad (x, y) \text{ in the quantum well} \\ 0, \qquad \text{otherwise} \end{cases} \quad (11)$$

$$s(x, y) \equiv \frac{E_f(x) - E_c(x, y)}{kT(x)} \quad (12)$$

$$H(u, s) \equiv \int_u^\infty \frac{w^{1/2} - u^{1/2}}{1 + \exp(w - s)}\,dw. \quad (13)$$

For electrons outside the InGaAs quantum well, u is zero by definition and $H(u, s)$ reduces to the familiar Fermi–Direct integral $F_{1/2}(s)$. In (13), we modified the density of states and the integration lower bound in the Fermi–Direc integral for the 3D bulk electrons in the InGaAs layer to avoid double-counting of the 2DEG density. Once $n(x, y)$ is known, the sheet concentration of the conducting electrons in the channel n_s is obtained by a simple integration

$$n_s(x) = \int_{\text{well}} n(x, y)\,dy. \quad (14)$$

In the MODFET structures, the AlGaAs layers are usually heavily doped so that the donor neutralization effects become crucial at a large gate bias. Neglect of the donor neutralization effects in the previous models [18] may cause a severe overestimate of the drain current. In this work, the ionized donor density N_D^+ is evaluated using the Fermi–Dirac statistics.

At the end of this section, we would like to mention that the 1D approximation of the Schrödinger equation is justified in the InGaAs pseudomorphic MODFET structures since the potential variation in the perpendicular direction due to the bandgap discontinuities is much more abrupt than the potential variation in the channel direc-

tion. This situation is unlike the AlGaAs/GaAs MODFET's in which the quantum confinement may disappear in the high-field region of the channel.

III. Simulation Methods

To solve all of the above mentioned equations self-consistently, a numerical algorithm illustrated in Fig. 6 is developed. An successive underrelaxation (SUR) scheme has been employed to damp all corrections of the variables in the program to avoid violent numerical fluctuations in iterations.

In the simulation, a nonuniform rectangular mesh is chosen to discretize the device under consideration. In order to have the boundary conditions of the electron sheet concentration at the source and drain ends for the transport calculations, the Schrödinger equation and the 1D Poisson equation along the y direction are first evaluated using the Neumann conditions for the potential at both upper and lower surfaces of the device.

In the quantization part, (5) is solved at each x grid line to give $e_i(x)$ and the normalized $\psi_i(x)$ by a numerical method similar to that used in [23]. Then, the quasi-Fermi level $E_f(x)$ is calculated from a binary search such that $n_s(x)$ calculated by (8)–(14) is equal to the value obtained from the transport equations.

The 2D Poisson equation, i.e., (7) with $N_D^+(x, y)$ calculated from the Fermi–Dirac distribution, is solved using the Incomplete Cholesky-Conjugate Gradient (ICCG) algorithm [24]. The convergence criterion for the potential in the ICCG routine is set equal to 10^{-5} V. Every time after the program passes its inner loop convergent criteria (see Fig. 6), the potential distribution is used to derive the electric field distribution for the transport calculation.

In the transport part, the balance equations are solved sequentially. Since the balance equations are 1D partial differential equations, a direct solution method (tri-diagonal method [25]) is available. Equations (1) and (2) are combined into

$$\frac{\partial}{\partial x}\left[\frac{q\tau_m'(E)}{m^*} n_s F\right] - \frac{k\tau_m'(E)}{m^*}\frac{\partial^2}{\partial x^2}(n_s T) = 0 \quad (15)$$

where

$$\tau_m'(E) \equiv \left[\frac{1}{\tau_m(E)} + \frac{\partial v}{\tau x}\right]^{-1}. \quad (16)$$

Equation (15) is a second-order differential equation of $n_s(x)$. Given $F(x)$, $T(x)$, and $\tau_m'(E(x))$, $n_s(x)$ can be easily solved by the tri-diagonal method using the boundary conditions discussed previously. The electron velocity profile $v(x)$ and $\partial v/\partial x$ in (16) are then updated using this $n_s(x)$ solution by

$$v(x) = \frac{q_m'(E)}{m^*} F - \frac{k\tau_m'(E)}{n_s m^*}\frac{\partial}{\partial x}(n_s T). \quad (17)$$

Similarly, we can derive a second-order differential equation for $T(x)$. Using a static field–temperature relationship at the source and data contacts as boundary conditions, we can obtain new $T(x)$ and correspondingly new $E(x)$ by the tri-diagonal method. The functions of $\tau_m(E)$ and $\tau_e(E)$ are stored in the computer program as a tabular form. A linear interpolation technique is utilized to calculate new $\tau_m'(E)$ and $\tau_e'(E)$ in (15). Successively, n_s, v, and T are corrected each iteration with a relaxation factor of 0.1 until the convergence criteria are satisfied under the current field profile. The small relaxation factor chosen here is to ensure the convergence stability and has not been optimized yet. The convergence tolerance for the transport equations is 10^{-4} relative change in n_s, v, and T. After the program passes the transport equations in the inner loop, the self-consistent n_s and T solutions are then put in the Schrödinger and the Poisson equations again to generate a new field profile in the next outer loop iteration (see Fig. 6). The iteration process continues until all governing equations are self-consistently solved.

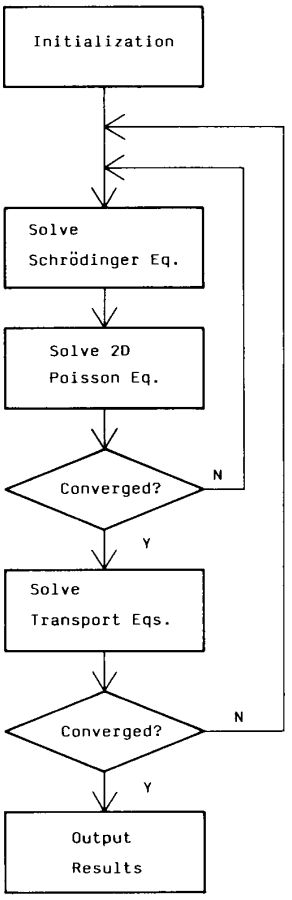

Fig. 6. Numerical algorithm for the pseudomorphic MODFET simulation.

IV. Results and Discussions

In this section, we would like to discuss the simulation result for a half-micrometer gate $In_{0.15}Ga_{0.85}As$ pseudomorphic MODFET at room temperature. The simulation is performed at a drain bias of 1.0 V and a gate bias of

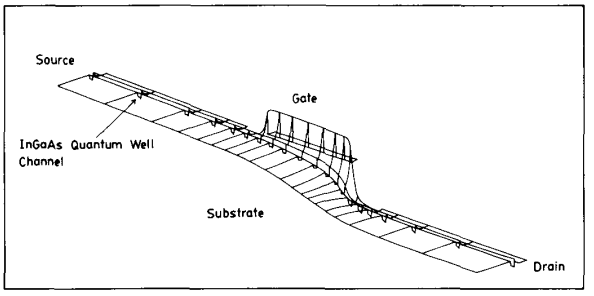

Fig. 7. A self-consistent two-dimensional band-edge diagram of the simulated pseudomorphic structure at a drain bias of 1.0 V and a gate bias of 0.0 V.

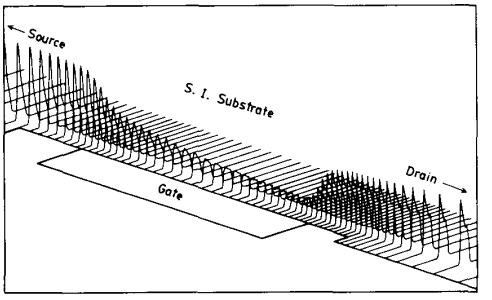

Fig. 8. Two-dimensional distribution of the electron concentration in the simulated device. Only the portion of the device close to the gate is shown.

0.0 V. The device configuration and material parameters are listed in Table I.

Fig. 7 is the calculated 2D conduction band-edge profile. This figure is drawn with the same scale in both x and y directions so that one can envision the quantum well in scale. Indeed, the quantum well is sufficiently thin that we can neglect the variation of the channel field in the y-direction in the quantum well and justify the 1D approach to the transport equations. Fig. 8 shows the 2D distribution of the conducting electrons $n(x, y)$ in the simulated device. In the source access region, the electron concentration has a δ-function-like distribution. The peak of the 2D electrons distribution is about 40 Å from the AlGaAs/InGaAs interface. The density function becomes more uniformly distributed under the gate. The reason is that the 2D electrons are heated by a large field and most of them are excited to higher states where the electrons have more spread wave functions. The distribution of the 2D electrons in the quantum well has intimate influence on the operation of the device. In this respect, the adoption of the 2D Poisson equation and the 1D Schrödinger equation simultaneously in the present model marks a major improvement over other existing MODFET models; For example, the 2D hydrodynamic model proposed by Widiger *et al.* [18] assumes a δ-function distribution of the 2D electrons exactly at the heterointerface. This assumption ignores the distance between the 2D electrons and the heterointerface and apparently exaggerates the charge-modulation capability from the gate. On the other side, the 1D models employed by many people [5], [6] include only the 1D Poisson equation and the 1D Schrödinger equation. Due to the neglect of the potential variation in the channel direction, the 1D Poisson equation tends to overestimate the repulsive field in the perpendicular direction under the gate. This in turn leads to the 2D electrons accumulation closer to the bottom interface (InGaAs/GaAs) in the pseudomorphic MODFET's, in other words, a larger distance from the gate to the 2D electrons. From this viewpoint, an underestimate of the gate capacitance is expected from the 1D models.

The longitudinal electric field in the quantum well is plotted as a function of distance in Fig. 9. The field is

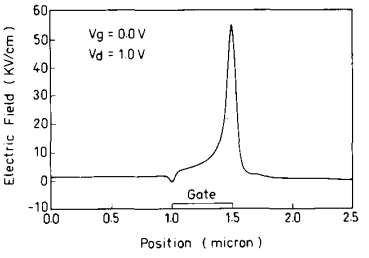

Fig. 9. Longitudinal electric field in the quantum well versus distance along the channel.

TABLE I
DEVICE AND MATERIAL PARAMETERS EMPLOYED IN THE SIMULATION

Source to Gate Spacing	1.0	μm
Drain to Gate Spacing	1.0	μm
Gate Length	0.5	μm
GaAs Buffer Layer Thickness	2000	Å
InGaAs Layer Thickness	200	Å
Undoped AlGaAs Spacer Layer Thickness	30	Å
AlGaAs Layer Thickness (Recessed Region)	380	Å
AlGaAs Layer Thickness (Unrecessed Region)	800	Å
AlGaAs Layer Doping Concentration	1.0×10^{18}	$1/cm^3$
Al Mole Fraction in AlGaAs Layer	0.15	
AlGaAs Electron Effective Mass	0.0795	m_0
InGaAs Electron Effective Mass	0.0556	m_0
AlGaAs/InGaAs Conduction Band Discontinuity	0.224	eV
InGaAs/GaAs Conduction Band Discontinuity	0.100	eV
Schottky Barrier Height	0.8	eV
Donor Level in AlGaAs Layer	6.0	meV
AlGaAs Dielectric Constant	12.39	ϵ_0
InGaAs Dielectric Constant	12.94	ϵ_0
GaAs Dielectric Constant	12.66	ϵ_0

highly nonuniform and exhibits a peak value of 56 kV/cm under the gate as a consequence of the pinch-off effect.

Fig. 10 plots the concentration distribution of the conducting electrons in the channel and Fig. 11 shows the

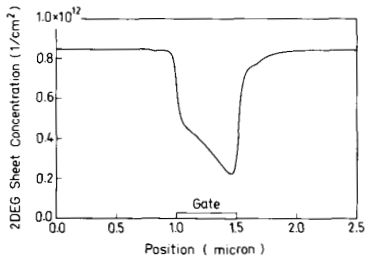

Fig. 10. Distribution of the conducting electron concentration along the channel.

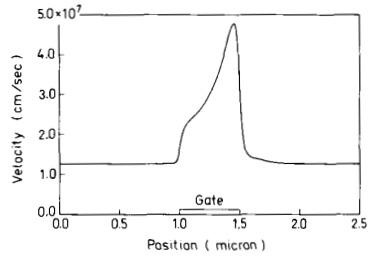

Fig. 11. Electron velocity distribution as a function of distance in the InGaAs channel.

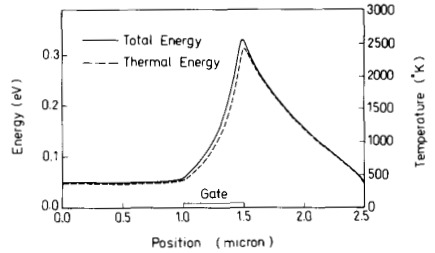

Fig. 12. Distributions of electron temperature and average energy along the channel.

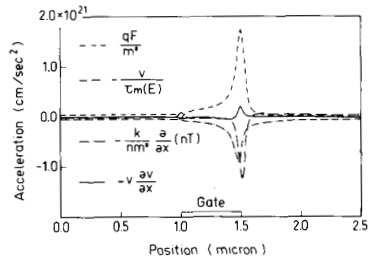

Fig. 13. Magnitudes of the individual terms in the momentum balance equation as functions of position in the InGaAs channel.

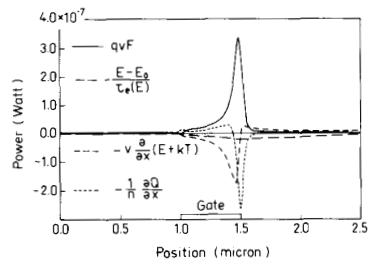

Fig. 14. Magnitudes of the individual terms in the energy balance equation as functions of position in the InGaAs channel.

electron velocity distribution. The result indicates a substantial velocity overshoot. The peak electron velocity exceeds 4.0×10^7 cm/s which is far above the steady-state saturation velocity balanced locally with the field in the InGaAs material. This result is consistent with the Monte Carlo calculations by Wang *et al.* [8] and Park *et al.* [9] and explains the eminently nice high-frequency characteristics of the pseudomorphic MODFET's.

Fig. 12 gives the calculated profiles of electron temperature and energy in the channel. At the sharp electric field spike, the electron temperature is as hot as 2500 K. The corresponding average electron energy reaches 0.3 eV above the conduction band minimum. This implies that the real-space transfer, as well as the k-space transfer, is likely to occur in the high-field region.

In Figs. 13 and 14, we evaluate the significance of each individual term in the momentum and energy transport equations respectively.

In the source access region, the electron transport is in fact very similar to that in an ordinary resistor (qF/m^* and $v/[\tau_m(E)]$ dominant as shown in Fig. 13). The carriers are drifted by the field with an average velocity of 1.3×10^7 cm/s and a temperature of about 370 K until they travel to the region under the gate.

The electric field becomes much stronger and increases rapidly with x under the gate. Electron momentum gained from the field is balanced by i) the momentum reduction due to the scatterings, ii) the retarding force resulted from the gradient of the electron gas pressure, and iii) the acceleration of the electron velocity. In Fig. 13, we observe that the momentum reduction due to the scatterings dominates in the low-field region under the gate, while the pressure gradient is more important at the high-field spike. In the conventional transport model, electron temperature is not retained inside the gradient operator in (2). Thus the effects of the pressure gradient reduce to the classical concept of diffusion. Using this simplification, one predicts a diffusion current in the same direction as the drift current under the gate. However, in our hot-electron model, the electrons are found to diffuse against the field drift under the gate. This is evidenced by the opposite direction of

$$\left(\frac{qF}{m^*}\right) \quad \text{and} \quad \left(-\frac{k}{n_s m^*}\frac{\partial}{\partial x}(n_s T)\right)$$

in Fig. 13. Upon entering the gate region, much momentum gained from the pressure gradient is used to accelerate electrons and the acceleration term $[-v\,(\partial v/\partial x)]$ takes about 40% of the scattering term $(v/\tau_m(E))$. On the contrary, electrons leaving the gate region decelerate and release some momenta due to the phonon scattering,

thus causing a positive peak on the $[-v(\partial v/\partial x)]$ curve in Fig. 13.

In Fig. 14, it is clear that only a small fraction of the field heating power is relaxed locally via scattering processes in the region under the gate. At the high-field spike, the excess power is "pumped" out by the gradient of the diffusive energy flux to the low-field region nearby. This effect is not included in the models based on a drifted Maxwellian distribution function. The Monte Carlo simulation by Wang and Hess [8] indicates that the distribution function in high-field region does exhibit a strong asymmetry. The Q term in (3) of our model describes the effects of this asymmetry and is found to have a great contribution to the total energy flow. The other part of the energy flow is the convective component $n_s v(E + kT)$ which carries a large amount of electron energy from the low-field region under the gate to the drain access region as shown in Fig. 14. Under the gate, the average electron energy is kept relatively low due to the energy flow gradient. This reduces the scattering rate and leads to the important consequence of space velocity overshoot.

In the drain access region, although the electron velocity is almost the same as in the source access region, the picture of carrier transport is quite different from that in the source access region. Because a large electron temperature gradient exists in this region of the device, electron transport is mainly achieved by the "hot diffusion" rather than by the field drift

$$\left(\frac{k}{n_s m^*}\frac{\partial}{\partial x}(n_s T) \quad \text{and} \quad \frac{v}{\tau_m}(E) \text{ dominant}\right).$$

The momentum dissipation by the scatterings is provided by the pressure gradient, while the energy dissipation due to the collisions is supplied from both the convective and the diffusive energy flux gradients.

The simulated device I-V characteristics is shown in Fig. 15. The transconductance at $V_g = 0.0$ V and $V_d = 1.0$ V can be extracted from the figure as 390 mS/mm. Notice that the knee voltage of the I-V curves is around 0.4 V due to the low parasitic resistance in the access regions. Current transport in the AlGaAs layer is not taken into account in the simulation. The influence of the DX centers is also not considered since the aluminum composition in the simulated structure is 0.15.

V. Conclusions

As a conclusion, we have developed a hot-electron model including both the effects of the 2D quantization and the nonequilibrium transport in the AlGaAs/InGaAs/GaAs pseudomorphic MODFET's. A significant overshoot of electron velocity under the gate is observed. The results of this work indicates that the classical assumption of a local and instantaneous balance between the electric field and carrier energy is not appropriate to describe the electron transport behaviors in the submicrometer MODFET devices.

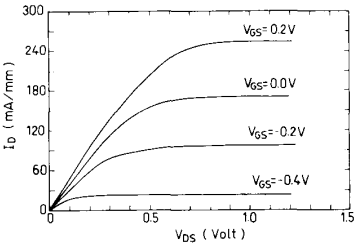

Fig. 15. Full device I-V characteristics of the pseudomorphic MODFET.

References

[1] L. D. Nguyen, W. J. Schaff, P. J. Tasker, A. N. Lepore, L. F. Palmateer, M. C. Foisy, and L. F. Eastman, "Charge control, dc, and RF performance of a 0.35-μm pseudomorphic AlGaAs/InGaAs modulation-doped field-effect transistor," *IEEE Trans. Electron Devices*, vol. 35, pp. 139-143, Feb. 1988.

[2] T. J. Maloney and J. Frey, "Transient and steady-state electron transport properties of GaAs and InP," *J. Appl. Phys.*, vol. 48, pp. 781-787, 1977.

[3] J. P. Nougier, J. C. Vaissiere, D. Gasquet, J. Zimmerman, and E. Constant, "Determination of transient regime of hot carriers in semiconductors, using the relaxation time approximation," *J. Appl. Phys.*, vol. 52, pp. 825-832, 1981.

[4] N. Moll, M. R. Hueschen, and A. Fischer-Colbrie, "Pulse-doped AlGaAs/InGaAs pseudomorphic MODFET's," *IEEE Trans. Electron Devices*, vol. 35, pp. 879-885, July 1988.

[5] Y. Ando and T. Itoh, "Analysis of charge control in pseudomorphic two-dimensional electron gas field-effect transistors," *IEEE Trans. Electron Devices*, vol. 35, pp. 2295-2301, Dec. 1988.

[6] H. Rohdin and P. Roblin, "A MODFET dc model with improved pinchoff and saturation characteristics," *IEEE Electron Devices*, vol. ED-33, pp. 664-672, May 1986.

[7] D. Loret, "Two-dimensional numerical model for the high electron mobility transistor," *Solid-State Electron.*, vol. 30, pp. 1197-1203, 1987.

[8] T. Wang and K. Hess, "Calculation of the electron velocity distribution in high electron mobility transistor using Monte Carlo method," *J. Appl. Phys.*, vol. 57, no. 12, pp. 5336-5339, 1985.

[9] D. Park, Y. Wang, and K. Brennan, "Ensemble Monte Carlo simulation of a 0.35-μm pseudomorphic HEMT," *IEEE Electron Device Lett.*, vol. 10, pp. 107-110, Mar. 1989.

[10] W. Stratton, "Diffusion of hot and cold electrons in semiconductor barriers," *Phys. Rev.*, vol. 126, no. 6, pp. 2002-2013, June 1962.

[11] K. Bløtekjaer, "Transport equations for electrons in two-valley semiconductors," *IEEE Trans. Electron Devices*, vol. ED-17, pp. 28-47, Jan. 1970.

[12] G. Baccarani and M. R. Wordeman, "An investigation of steady-state velocity overshoot in silicon," *Solid-State Electron.*, vol. 28, no. 4, pp. 407-416, 1985.

[13] R. K. Cook and J. Frey, "Diffusion effects and ballistic transport," *IEEE Trans. Electron Devices*, vol. ED-28, pp. 951-953, Aug. 1981.

[14] C. M. Snowden and D. Loret, "Two-dimensional hot-electron models for short-gate-length GaAs MESFET's," *IEEE Trans. Electron Devices*, vol. ED-34, pp. 212-223, 1987.

[15] Y. Feng and A. Hintz, "Simulation of submicrometer GaAs MESFET's using a full dynamic transport model," *IEEE Trans. Electron Devices*, vol. 35, pp. 1419-1431, Sept. 1988.

[16] F. J. Blatt, *Physics of Electronic Conduction in Solids*. New York, NY: McGraw-Hill, 1968.

[17] B. R. Nag, "Electron transport in compound semiconductors," in *Springer Series in Solid-State Science*, vol. 11. Berlin, Heidelberg, New York: Springer-Verlag, 1980, p. 174.

[18] D. Widiger, K. Hess, and J. J. Coleman, "Two-dimensional simulation of the high electron mobility transistor," *IEEE Electron Device Lett.*, vol. EDL-5, pp. 266-269, 1984.

[19] E. M. Azoff, "Generalized energy-momentum conservation equations in the relaxation time approximation," *Solid-State Electron.*, vol. 30, no. 9, pp. 913-917, 1987.

[20] K. F. Brennan and D. H. Park, "Theoretical comparison of electron real-space transfer in classical and quantum two-dimensional het-

erostructure systems," *J. Appl. Phys.*, vol. 65, no. 3, pp. 1156–1163, 1989.
[21] K. Yokoyama and K. Hess, "A Monte Carlo study of electronic transport in AlGaAs/GaAs single-well heterostructures," *Phys. Rev. B*, vol. 33, no. 8, pp. 5595–5606, 1986.
[22] F. Stern and S. D. Sarma, "Electron energy levels in GaAs-$Ga_{1-x}Al_xAs$ heterojunctions," *Phys. Rev. B*, vol. 30, pp. 840–848, July 1984.
[23] F. Stern, "Iteration method for calculating self-consistent fields in semiconductor inversion layers," *J. Comp. Phys.*, vol. 6, p. 56, 1970.
[24] D. S. Kershaw, "The incomplete Cholesky-conjugate gradient method for the iterative solution of systems of linear equations," *J. Comp. Phys.*, vol. 26, pp. 43–56, 1978.
[25] C. F. Gerald, *Appled Numerical Analysis*. Reading, MA: Addison-Wesley, 1978, p. 129.

*

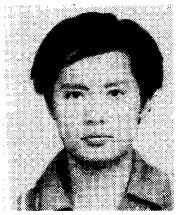

Tahui Wang was born in Taoyuan, Taiwan, on May 3, 1958. He received the B.S. and Ph.D. degrees in electrical engineering from the National Taiwan University and the University of Illinois in 1980 and 1986, respectively.

From 1985 to 1987, he was with the High-Speed Devices Laboratory of Hewlett-Packard Laboratories, where he was engaged in research and development of compound semiconductor devices and circuits. Currently, he is an associate professor at the Institute of Electronics, National Chiao-Tung University. His current research interest is in the modeling and simulation of high-speed semiconductor devices and circuits.

*

Cheng-Hsiang Hsieh was born on January 2, 1963, in Taipei, Taiwan. He received the B.S. and M.S. degrees in electrical engineering from the National Cheng-Kung University and the National Chiao-Tung University in 1985 and 1989, respectively.

He is currently employed as a circuit designer by Winbond Electronics Corp. His major research interests include submicrometer devices transport and modeling and memory circuit design.